4-1-2021

Bio-printed, bio-functionalized PLGA-KGN scaffolds as an augmentation to microfracture

James D. Warren
Mississippi State University

Bio-printed, bio-functionalized PLGA-KGN scaffolds as an augmentation to microfracture

By

James Darrah Warren

Steve Elder	Lauren Priddy
Professor	Assistant Professor
(Director of Thesis)	(Committee Member)

LaShan Simpson

Associate Professor & Coordinator of Diversity Initiatives

(Shackouls Honors College Representative)

Honors Thesis submitted to Shackouls Honors College, Mississippi State University, Spring 2021

Bio-printed, bio-functionalized PLGA-KGN scaffolds as an augmentation to microfracture

By

James Darrah Warren

Approved by:

Steve Elder (Major Professor)
Lauren Priddy
LaShan Simpson

A Thesis
Submitted to the Faculty of
Mississippi State University
in Partial Fulfillment of the Requirements
for the Degree of Bachelor of Science
in Biomedical Engineering
in the Department of Agricultural and Biological Engineering

Mississippi State, Mississippi

April 2021

Name: James Darrah Warren

Date of Degree: April 30, 2021

Institution: Mississippi State University

Major Field: Biomedical Engineering

Major Professor: Dr. Steve Elder

Title of Study: Bio-printed, bio-functionalized PLGA-KGN scaffolds as an augmentation to microfracture

Pages in Study: 44

Candidate for Degree of Bachelor of Science

Microfracture is a commonly performed surgical procedure that aims to regenerate damaged cartilage in patients with focal cartilage lesions. Though fairly successful, microfracture is limited by the produced fibrocartilage, which is mechanically inferior and less durable than normal hyaline cartilage. The proposed augmentation to microfracture aims to improve its clinical outcomes by introducing a bio-printed poly(lactic-co-glycolic acid) (PLGA) scaffold functionalized with kartogenin (KGN), a small bioactive molecule known to induce mesenchymal stem cell differentiation into hyaline cartilage. The scaffold's release characteristics were evaluated over 40 days by HPLC, which confirmed sustained release of KGN from the scaffold. Tensile testing results indicate that PLGA functionalization with KGN has no significant impact on PLGA's elastic modulus or tensile strength, but it does significantly increase the polymer's overall toughness. Overall, this method of scaffold fabrication and functionalization is a very viable option for delivering KGN to cartilage defect sites immediately after microfracture.

DEDICATION

To my family and friends for their constant love and support.

ACKNOWLEDGEMENTS

This work has been supported by funds from the Judy and Bobby Shackouls Honors College. I would like to express my gratitude to those individuals within the Honors College who serviced the effort to make this work possible.

To Professor Steve Elder, for agreeing to serve as the major professor and offering mentorship, guidance, and wisdom throughout my undergraduate studies.

To Weitong Chen, for his unparalleled knowledge and exceptionally patient instruction in bioprinting.

To Dr. Matthew Ross and Daniel Young, whose expertise in HPLC and LC-MS contributed greatly to this project.

To Dr. Lauren Priddy and Dr. LaShan Simpson, for serving as the internal and Honors committee members and emboldening the academic success of their students.

To Dr. Anastasia Elder, for providing guidance and direction throughout the Honors Thesis process.

TABLE OF CONTENTS

LIST OF TABLES

LIST OF FIGURES

CHAPTER I

INTRODUCTION

1.1 Articular Cartilage Lesions

Articular cartilage is a viscoelastic material responsible for load bearing in joints. Articular cartilage covers underlying subchondral bone, minimizing stress on subchondral bone and reducing bone-bone friction. Cartilage is made up of chondrocytes, water, and a matrix component, which is primarily composed of Type II collagen and some proteoglycans. The collagen fibers are arranged in a lattice framework, which provides cartilage its structural stability and resilience.[1]

Articular cartilage lesions are broadly classified as injuries in which the articular cartilage of a joint is damaged, such as a tear or a fracture. These lesions can be caused by a number of factors, from joint dislocation and subluxation to chronic cartilage degeneration. Articular cartilage lesions vary in their location and severity and are classified accordingly. The most commonly used classification system for cartilage lesions is the grading system devised by Outerbridge[2], shown in Figure 1.1.[3] Regardless of severity, articular cartilage lesions are often unable to heal on their own due to their lack of vasculature and thus their inability to supply regenerative chondrocytes to damaged areas.[1]

Articular cartilage lesions are fairly common in the population and are often symptomatic. A review of 25,124 knee arthroscopies revealed that an isolated cartilage lesion was discovered in 18% of patients.[4] Focal cartilage and osteochondral injuries have profound detrimental impacts on patients' quality of life due to the associated pain and functional impairment.[5] Besides pain,

symptoms include crepitus, effusion, and joint locking.[6] Symptomatic patients generally require surgical treatment because of the limited intrinsic repair capacity of articular cartilage.

Articular cartilage lesions are especially problematic in the knee joint due to its distinct anatomy and distribution of external forces. As the central joint of the lower extremity, the knee is comprised of four bones: the femur, patella, tibia, and fibula. The knee also features a complex arrangement of muscles, tendons, and ligaments. The knee's range of motion relies on the tibiofemoral articulation, the patellofemoral articulation, and the tibiofibular articulation. This normal range of motion is reliant on healthy articular cartilage covering the tibia, femur, and patella.[1] Chondral lesions on the knee can impair range of motion and cause pain and stiffness in patients. Since articular cartilage is unable to heal itself, these lesions also have a propensity to progress to the early stages of osteoarthritis.

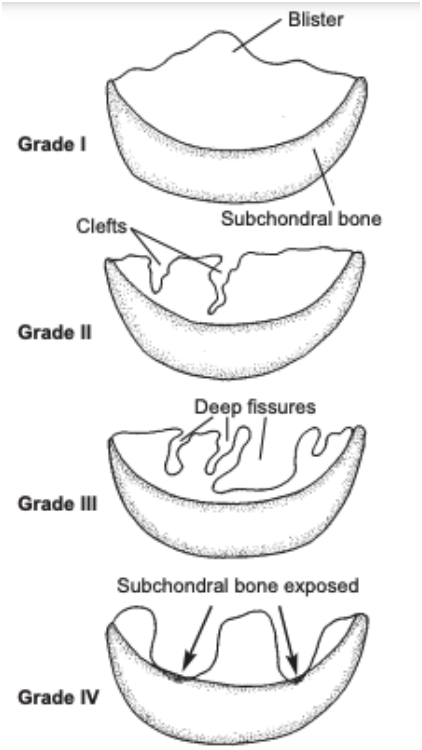

Figure 1.1 Visual depiction of the Outerbridge[2] grading system of articular cartilage lesions.[3]

1.2 Osteoarthritis

Osteoarthritis (OA) is a degenerative joint disease that affects articular cartilage and surrounding joint tissues. OA is a chronic condition that slowly removes articular cartilage from joints, which impacts joint movement, lubrication, and support. Symptoms of osteoarthritis include joint pain, stiffness, and limited range of motion.[7]

Osteoarthritis can occur anywhere in the body, but the most common locations include the hand, hip, and knee. OA impacts over 70% of America's population between the ages of 55 and 70, and over 25 million Americans are estimated to have some form of the disease.[7,8] Though there is a lack of consensus on known causes of osteoarthritis, studies have identified a variety of systemic and local risk factors.

One of the most well-established risk factors for OA is obesity. Some studies propose that OA is associated with the metabolic syndrome, which could suggest that OA is involved in this fairly common pathogenic mechanism. Similarly, cardiovascular disease, such as hypertension, has been associated with a higher predisposition for OA. Age also plays a factor, as the prevalence of OA in the population increases substantially with age. There is a higher incidence of knee, hand, and hip OA in women than in men, and in women the incidence of OA increases dramatically post-menopause, suggesting a possible hormonal exacerbator in its development.[7] There is also a strong genetic influence on a patient's predisposition to the development of OA, though the exact genetic mechanisms are unknown.[9]

Traumatic joint injuries are also a major risk factor for the development of OA. Acute bone fractures and dislocations can increase the risk of OA development. Similarly, tears in a joint's surrounding ligaments and/or tendons can impact the overall stability of the joint, potentially causing joint degeneration.[9] Workers who work in environments where they are subjected to excessive, repetitive weight loading are also at an increased risk.[7]

Articular cartilage lesions are a major risk factor in the development of osteoarthritis. According to a study by Ding, et al.,[10] significant knee cartilage defects serve as a predictor of cartilage loss over a 2-year period. A similar study indicates that grade 3 medial tibial cartilage defects are predicted to progress to end-stage OA within 17 years after a projected 60% decrease in cartilage.[11] Though the exact pathogenesis of this progression is unknown, it is likely that cartilage lesions induce an inflammatory swelling of knee cartilage (due to early-stage OA), resulting in an increase in knee cartilage volume and a subsequent increase in cartilage defect size.[10] In other words, once the early stages of osteoarthritis have begun, there is a resultant exacerbation of existing cartilage lesions.

Osteoarthritis largely impacts the quality of life of patients with the disease. The effects of osteoarthritis can be incredibly burdensome for some patients, especially in cases where OA affects weight-bearing joints. The pain, stiffness, and lack of mobility that is associated with OA can often lead to disability, with many patients requiring surgical intervention to improve their quality of life.

1.3 Microfracture and Its Limitations

One of the most commonly performed surgical procedures for the restoration of damaged cartilage is microfracture. Microfracture has been shown clinically to be effective at repairing full-thickness cartilage lesions, and its cost-effective and relatively uncomplicated procedure makes it a safe choice for many patients.[12–14] Developed in the early 1980s, the goal of the procedure is to use an awl to produce small "microfractures" in the subchondral bone of full-thickness cartilage lesions. Compared to cartilage's avascular nature, bone is vascular. By producing small microfractures in the subchondral bone of lesion sites, blood from the bone is recruited to the defect site. This blood contains marrow-derived progenitor cells and growth factors that can aid in cartilage regeneration.[12] Once the blood forms a clot on the rough surface created by the awl perforations, an acute inflammatory response is stimulated and vascularized granulation tissue is created. Over a period of about 8 weeks, the mesenchymal stem cells (MSCs) recruited during the procedure can differentiate into fibrocartilage, thereby repairing the cartilage lesion.[15] A visual depiction of microfracture is shown in Figure 1.2.

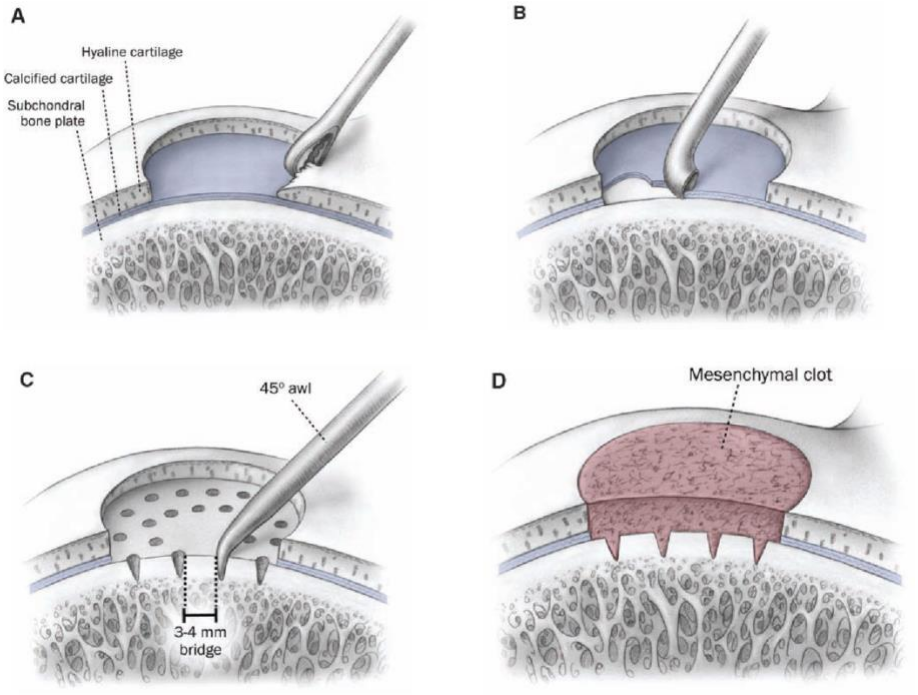

Figure 1.2 Visual depiction of microfracture procedure.[13]

One limitation of microfracture is the fact that the generated cartilage tissue is composed primarily of fibrocartilage, rather than the hyaline cartilage normally found within joints. Compared to hyaline cartilage, fibrocartilage is mechanically inferior and easily degraded. The reason for this discrepancy is largely based on each tissue's collagen composition. Whereas type II collagen represents 90-95% of the collagen in hyaline cartilage, fibrocartilage consists of predominantly type I collagen (commonly found in skin, bone, ligaments, and tendons) and has less than half the compressive stiffness of hyaline cartilage.[16] Marrow stimulation-induced repair tissue is also deficient in proteoglycan[17], well known for its important contribution to the compressive resistance of cartilage. Due to its mechanical limitations, microfracture is considered

to be a good treatment option only for lesions smaller than 2 cm^2.[18] It is contraindicated when the defect is larger than 4 cm^2.[19] Furthermore, a systematic review of 15 studies concluded that treatment failure after microfracture could be expected beyond 5 years postoperatively.[20] Thus, a fibrocartilaginous repair has limited durability.

1.4 Kartogenin and Its Influence on Chondrogenesis

A potential method of improving the efficacy of microfracture involves the directed differentiation of multipotent mesenchymal stem cells found within subchondral bone marrow. MSCs have the potential to differentiate into osteoblasts, fibroblasts, chondroblasts, and chondrocytes, with differentiation dependent upon cell signaling, environment, and other factors.

Kartogenin (KGN), a small bioactive molecule, has demonstrated an ability to aid in MSC differentiation into chondrocytes, the cells that form cartilage. KGN signaling directly results in chondrocyte-specific gene expression within MSCs, driving hyaline cartilage production over fibrocartilage tissue. Chondrocyte-specific gene expressions include Type II collagen, aggrecan, and lubricin, all of which demonstrate an up-regulation when MSC differentiation is directed by KGN (Fig. 1.3). This up-regulation of chondrocyte-specific gene expression alters the structural and mechanical properties of the resulting tissue to be superior to fibrocartilage.[8]

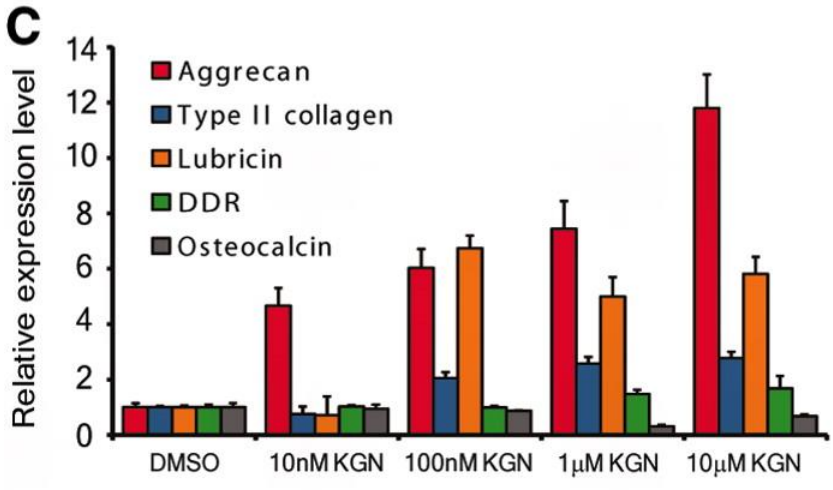

Figure 1.3 Up-regulation of chondrocyte-specific gene expression in hMSCs following 72-hour exposure to varying concentrations of KGN.[8]

It has previously been demonstrated that the modification of MSC cytoskeleton structure can induce chondrocyte differentiation.[21] A cytoskeleton is an internal collection of protein filaments that gives shape to cells and provides flexibility. Filamin A (FLNA) is an actin-binding protein located within cells that regulates the structure and organization of a cell's cytoskeleton. FLNA can also bind to other proteins both within and outside the cell, making it a valuable component in cell migration, adhesion, signaling, and survival. In a resting state, FLNA is bound to CBFβ, a subunit of the heterodimeric core-binding factor transcription complex. When CBFβ is activated, it releases from FLNA and migrates to the nucleus of the cell, where it binds to and activates the RUNX family of transcription factors. These transcription factors are considered to be involved in chondrogenesis, chondrocyte proliferation, and chondrocyte survival. KGN functions by binding to FLNA at the FLNA- CBFβ binding site. This activates CBFβ, which in turn activates RUNX transcription factors, resulting in an increased differentiation of MSCs into chondrocytes.[8]

1.5 PLGA Scaffolds as Vehicles for Drug Delivery

Within the realm of tissue engineering, the design and fabrication of synthetic bone substitutes, called scaffolds, presents a valuable alternative to the use of allografts, autografts, or xenografts.[22] Autografts are tissue grafts from a different part of a recipient's body, allografts are tissue grafts from a same-species donor, and xenografts are tissue grafts from another species entirely. Like any graft, scaffolds must present suitable characteristics for use in tissue regeneration, namely biocompatibility, bioactivity, and biodegradation.[23–25]

Though there are many materials used in the fabrication of scaffolds, biodegradable polymers represent some of the best options due to their appropriate physical, chemical, and biological properties. Biodegradable polymers can be naturally broken down by the body through enzymatic and/or non-enzymatic degradation. The by-products of this degradation are biocompatible and can be expelled by the body through its normal metabolic processes.[26] Biodegradable polymers can be classified as either natural or synthetic. Compared to natural polymers such as proteins, synthetic polymers tend to have several advantages, including a customizable degradation rate and consistent mechanical and physical properties.[23,24] Some of the most common synthetic polymers include polylactic acid (PLA), polyglycolic acid (PGA), and poly(lactic-*co*-glycolic) acid (PLGA) copolymers.

PLGA, formed through the combination of PLA and PGA, retains the suitable properties of PLA and PGA while demonstrating superior degradation control. PLGA is degraded in aqueous environments through hydrolytic de-esterification. Water in the body disrupts the van der Waals forces and hydrogen bonding found between adjacent atoms within PLGA. The covalent bonds within the polymer are cleaved, resulting in a decrease in molecular weight and the formation of carboxylic end groups. The carboxylic end groups then catalyze the PLGA degradation process,

cleaving covalent bonds in the polymer's backbone and decreasing PLGA's overall structural integrity.[23] The remaining fragments of PLGA are further cleaved into its PLA and PGA monomers. PLA and PGA are both converted to carbon dioxide and water via the tricarboxylic acid cycle. PGA can also be excreted unaltered by the kidney.[26] Figure 1.4 shows the chemical structure of PLGA and its monomers.

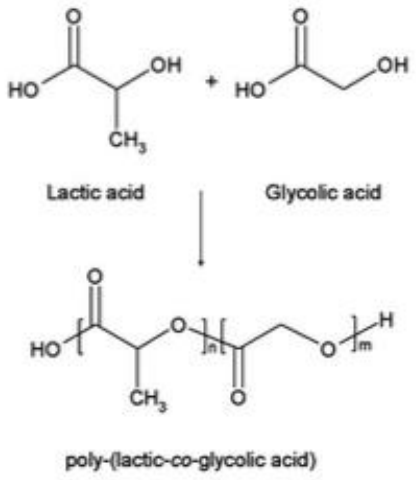

Figure 1.4 Chemical structure of poly(lactic-*co*-glycolic acid) and its monomers.[23]

One advantage of using PLGA as a scaffold material is its highly controlled and consistent degradation rate, which can be altered in a number of ways. Molecular weight of PLGA plays a large part in degradation, and a higher molecular weight results in a longer degradation period. The ratio of PGA to PLA in the PLGA polymer can also be modified to control its degradation (Fig. 1.5). In general, PLGA scaffolds with a higher PLA content are less hydrophilic, which means that they absorb less water and thus degrade more slowly. An exception to this rule is found in a 50:50 ratio of PGA to PLA, which demonstrates the fastest degradation period. End-group

functionalization can also prolong the degradation process. PLGA polymers with esters attached to its carboxylic acid end groups degrade more slowly than polymers with free carboxylic acid end groups. The shape of the scaffold also plays a large part in determining its degradation profile. Increased surface area of the scaffold (either through the introduction of a porous structure or a change in overall geometry) allows for greater water access, resulting in faster degradation times.[23]

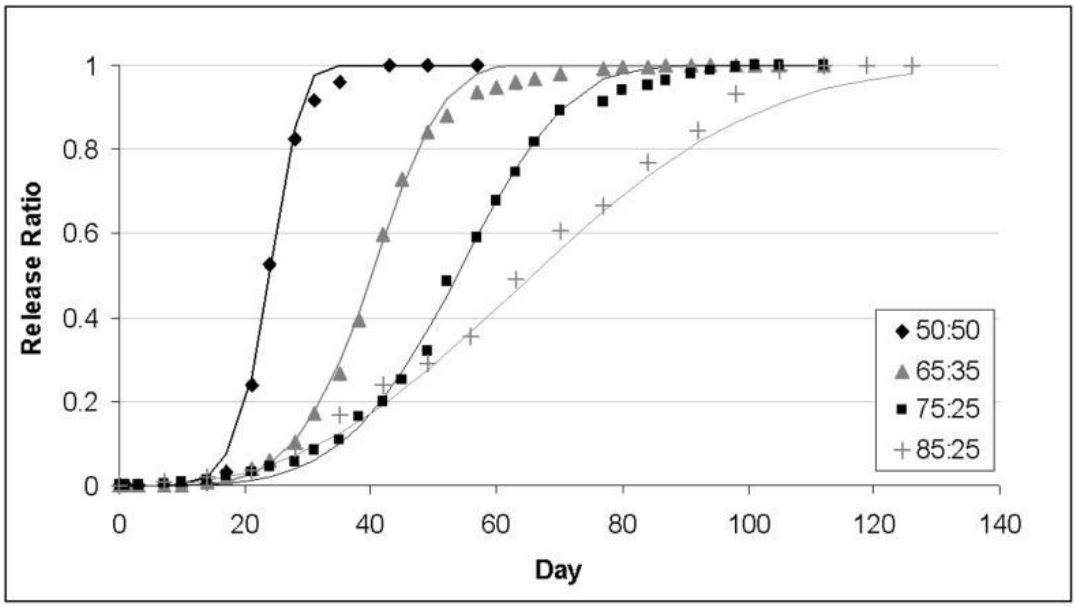

Figure 1.5 Modeled in vivo release profiles for 50:50, 65:35*, 75:25, and 85:15 poly(lactic-*co*-glycolic acid).[26]

*Note: notation of 65:35 PLGA means 65% of the copolymer is lactic acid and 35% is glycolic acid.

Drug release is closely tied to PLGA degradation, with individual release profiles dependent on a number of factors, such as drug solubility, loading concentration, drug hydrophobicity, etc. In any case, the resulting release profile of a drug can be considered a biphasic release. In the first stage of drug release, there is an initial burst of release of the drug from the polymer. The drug on the polymer surface has direct exposure to dissolving medium, and it

releases into the surrounding medium depending on the drug's level of solubility and hydrophobicity. In this stage, the covalent bonds within PLGA are beginning to shear, resulting in a decrease of molecular weight and an increase in free carboxylic end groups, yet no formation of PLA and PGA monomers. In the second stage of release, the drug is released slowly and is perhaps more reliant on the bulk degradation of PLGA. As the backbone of the PLGA structure is cleaved, the resulting PLA and PGA monomers are metabolized by the body, producing a channel for drug to be released into the surrounding medium through simple diffusion. This stage of release continues until PLGA has completely degraded and the drug has completely released.[26]

PLGA is used in a variety of tissue engineering applications, including the fabrication of porous scaffolds, hydrogels, and microspheres.[24] The versatility and predictable properties of PLGA allows for much creativity in designing novel methods of drug delivery. Notably, biodegradable synthetic polymers have recently been used to create 3D printed scaffolds functionalized with aggrecan.[27] This novel method of functionalizing bioactive molecules or other signaling molecules into a synthetic scaffold represents a promising approach to the regeneration of cartilage defects.

1.6 Proposed Augmentation to Microfracture Surgery

When microfracture surgery is performed, the standard recruitment of MSCs via small subchondral bone perforations results in the production of fibrocartilage, which is mechanically inferior to normal hyaline cartilage. This is one of microfracture's principal limitations, and one that could be solved through a minor augmentation to the existing procedure. The proposed augmentation would supplement the procedure with a 3D-printed PLGA scaffold that has been bio-functionalized with KGN. This scaffold would be attached to the defect site via fibrin glue once all subchondral bone perforations have been made. As PLGA naturally degrades in the body

over time, KGN will release in a controlled manner and diffuse into the joint to direct MSC differentiation into normal hyaline cartilage, thereby mitigating the principal limitation of microfracture.

Previously, microfracture technique has been used in conjunction with intra-articular injection of KGN with promising results.[28] However, this approach could be improved upon by introducing a controlled release component of KGN delivery. The use of PLGA as a scaffold material allows the release rate of KGN to be modified based on appropriate context. PLGA properties (PLA:PGA ratio, molecular weight, etc.) and scaffold properties (geometry, porosity, etc.) can be altered to accomplish a fine-tuned rate of KGN release.

The introduction of a PLGA-KGN scaffold to the existing microfracture procedure should have a substantial effect on the success of the operation. By using a synthetic 3D scaffold in tandem with a bioactive, chondro-inductive compound such as KGN, this tissue engineering solution will have prominent applications within the clinical realm to combat osteoarthritis. With this proposed augmentation of microfracture surgery, the procedure will finally provide an effective means of restoring normal, functional, hyaline cartilage to areas of degeneration and deficit.

CHAPTER II

PRELIMINARY STUDY OF PLGA-KGN SCAFFOLD FABRICATION

2.1 Overview

Similar scaffolds have been fabricated with aims to augment microfracture procedure and produce better clinical outcomes. Notably, aggrecan (the most abundant proteoglycan found within the extracellular matrix of articular cartilage) has been covalently bound to printed PLCL scaffolds via EDC-NHS crosslinking as a means of promoting hyaline cartilage regeneration after microfracture procedure.[27] In fact, there are a variety of scaffold functionalization methods that are performed post-printing. The proposed method of scaffold functionalization is somewhat unique in that it is reliant on simple admixing of KGN into PLGA to form a powder that is then used in bioprinting. This type of scaffold functionalization should promote a KGN release profile that is closely tied to PLGA's degradation in the body, rather than a release profile tied to the disruption of covalent interactions between PLGA and KGN.

A pilot study was conducted in order to determine the viability of this proposed method of PLGA-KGN scaffold fabrication. This preliminary study aimed to evaluate the loading efficiency of KGN into a PLGA-KGN powder, as well as KGN's ability to undergo the high temperatures and pressures associated with the fabrication and printing process.

2.2 Preliminary PLGA-KGN Powder Fabrication

Poly(lactic-co-glycolic acid) (PLGA, LACTEL, Birmingham, AL) with a PGA:PLA ratio of 50:50 and inherent viscosity of 1.03 dL/g was dissolved in dichloromethane (DCM, Sigma-Aldrich, St. Louis, MO) to create a 20% wt/vol solution. The dissolved PLGA was then combined with 0.25% (w/w) kartogenin (KGN, Shaanxi Dideu Medichem Co. Limited, China) that had first been dissolved in 1 mL dimethyl sulfoxide (DMSO, Fisher Chemical, Hampton, NH). The resulting PLGA-KGN mixture was stirred for 1 hour, then set in a fume hood overnight to evaporate the organic solvent. The next day, the mixture was heated at 75 ºC for 3-4 hours to evaporate any remaining solvent. The resulting solid was then ground to a powder for use in bioprinting.

2.3 Creation of Standard Curve (KGN Concentration vs Absorbance at 284 nm)

A standard curve (Fig. 2.1) was constructed in order to correlate KGN concentration to A284 absorbance. KGN underwent serial dilution in both PBS and DMSO, and absorbances of the known KGN concentrations were obtained via spectrophotometry at 284 nm (NanoDrop 2000c, Thermo Scientific, Waltham, MA). The resulting data was used to construct a standard curve. There was no observed effect of solvent choice on absorbance value.

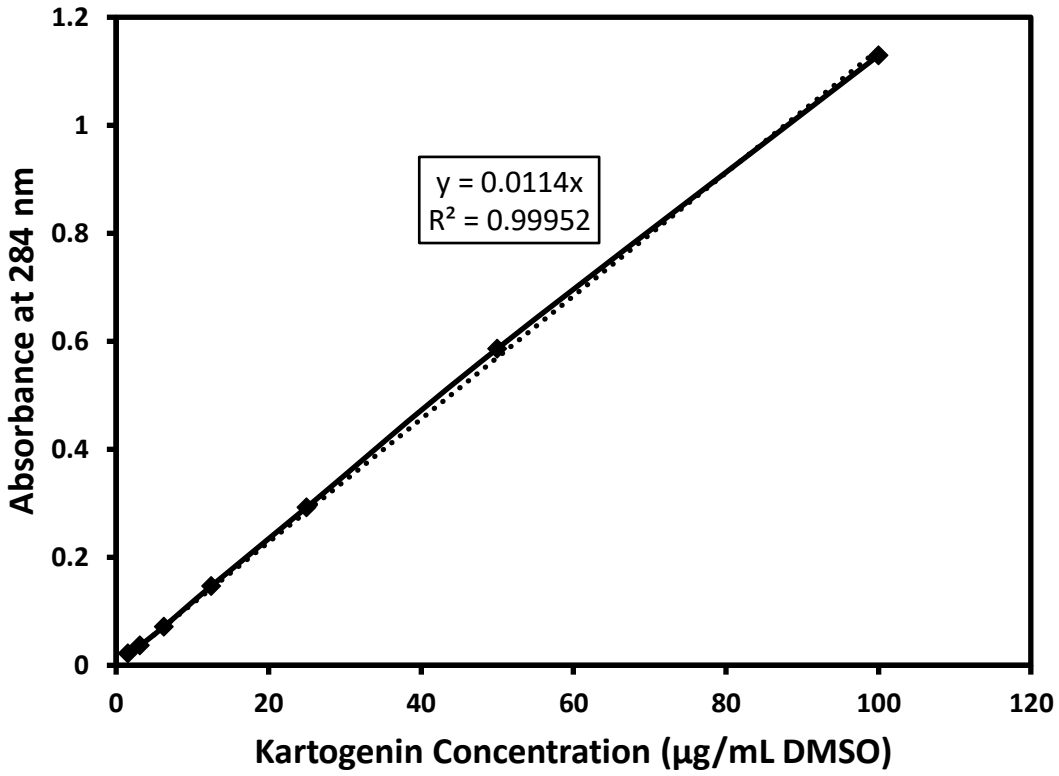

Figure 2.1 KGN Concentration vs A284 UV-Vis Absorbance

2.4 Evaluation of PLGA-KGN Powder Loading Efficiency

The preliminary PLGA-KGN powder was weighed and dissolved in DMSO, and the KGN concentration of the resulting solution was determined by spectrophotometry at 284 nm. This value was then used to calculate mass of KGN in solution. The loaded mass of KGN was calculated by using the 1:400 KGN:PLGA ratio used in fabrication, as well as the measured mass of the dissolved powder. Loading efficiency of KGN into the preliminary PLGA-KGN powder was then calculated by using Equation 1, shown below.

$$Loading\ Efficiency\ (\%) = \frac{Measured\ amount\ of\ dissolved\ KGN\ (g)}{Loaded\ amount\ of\ KGN\ (g)} \times 100 \quad (2)$$

Six loading efficiency trials were performed using the preliminary PLGA-KGN powder. Average loading efficiency was calculated to be 66%, indicating that 66% of the KGN originally mixed into the PLGA remained in the fabricated PLGA-KGN powder.

2.5 Bioprinting of Preliminary Scaffolds

Preliminary PLGA-KGN scaffolds were fabricated using the BioX bioprinter (CELLINK, Boston, MA). The scaffold's geometry (10 mm x 10 mm x 1 mm) was designed using SolidWorks 2019, and the inner pattern (rectilinear, 100% infill density, 0.33 mm layer height) was programmed using the BioX's integrated software. Preliminary PLGA-KGN powder was loaded into a metal cartridge and attached to a thermoplastic printhead. The print bed was lined with painter's tape to ensure adequate adhesion of the polymer. The loaded PLGA-KGN powder was melted at 105 ºC for 1 hr, then extruded at 92 kPa with an average speed of 3 mm/s using a 0.3 mm diameter nozzle. A pre-flow of 200 ms was also used during printing.

2.6 Loading Efficiency of Preliminary PLGA-KGN Scaffolds

A preliminary PLGA-KGN scaffold was weighed and dissolved in 5 mL DMSO, and the KGN concentration of the resulting solution was determined by spectrophotometry at 284 nm. This value was then used to calculate mass of KGN in solution. The loaded mass of KGN was determined by once again using a 1:400 KGN:PLGA ratio and the measured mass of the dissolved scaffold. Loading efficiency of KGN into preliminary PLGA-KGN scaffold was then calculated using Equation 1.

Based on the 158.4 mg mass of the printed scaffold, the theoretical loaded mass of KGN was determined to be 396.1 μg. The average UV-Vis absorbance at 284 nm was 0.5, which corresponds to a KGN concentration of 43.8 μg/mL and a KGN mass of 218.9 μg. Based on these values, loading efficiency of KGN into preliminary PLGA-KGN scaffolds was calculated to be 55.3%.

2.7 Discussion of Pilot Study Findings

The goal of this study was to determine the viability of the proposed method of scaffold functionalization. This was done by evaluating loading characteristics of KGN into PLGA at both the powder production and printing stages fabrication.

In evaluating the loading efficiency of PLGA-KGN powder, it was determined that KGN does in fact evenly distribute into a PLGA-KGN powder, as indicated by a fairly consistent 66% loading efficiency across six trials. KGN also retained its chemical stability after bioprinting of the PLGA-KGN powder into preliminary scaffolds, yielding a 55.3% loading efficiency. This indicates that KGN withstands the high temperatures associated with the bioprinting protocol, though the decrease in loading efficiency between powder production and bioprinting stages could suggest that some KGN is lost during the printing process.

Upon evaluation of the fabrication protocol used in preliminary study, at least one modification could be made in order to improve overall loading efficiency. After grinding the solid PLGA-KGN mixture into a powder, the powder was observed to be not entirely dry, suggesting that some solvent remained in the PLGA-KGN. This was further indicated by the powder's inconsistent bioprinting parameters. Whereas pure PLGA was determined to favor an extrusion temperature and pressure of 150 ºC and 400 kPa, respectively, the preliminary PLGA-KGN powder printed at a much lower temperature and pressure. The viscosity of the extruded material

was also much lower than that of pure PLGA, further indicating the presence of a liquid in the PLGA-KGN mixture. In examining the preliminary fabrication protocol, it was concluded that DMSO did not entirely evaporate (analysis of DMSO's material properties revealed an evaporation temperature of 189 ºC). It is hypothesized that the presence of DMSO in the solid PLGA-KGN mixture significantly lowered loading efficiency calculations and negatively impacted the material and printing properties of the PLGA-KGN powder. Future protocols add a step for DMSO evaporation, which should positively impact loading efficiency calculations and improve the bioprinting characteristics of the PLGA-KGN mixture. Alternatively, the protocol could replace DMSO with an organic solvent that evaporates at lower temperatures, such as ethyl acetate.

CHAPTER III

PLGA-KGN SCAFFOLD FABRICATION

3.1 Overview

Taking into account the findings of the preliminary study on PLGA-KGN scaffold fabrication, primary PLGA-KGN scaffolds were produced. KGN loading was also modified to reflect a therapeutic dose of KGN. Loading efficiency of KGN into PLGA-KGN scaffolds was calculated to determine the effect of a DMSO evaporation step added to the fabrication protocol.

3.2 Fabrication of PLGA-KGN Scaffolds

3.2.1 Determination of KGN Loading

KGN loading was altered to reflect the effective therapeutic KGN dose of 100 nM proposed by Johnson, et al.[8] Assuming that the printed PLGA-KGN scaffold will release into 15 mL of solution, the KGN loading mass was calculated to be 5 μg, as shown below.

Convert loaded mass of KGN mass to loaded mols KGN, then determine KGN concentration:

$$\frac{KGN\ load\ (g)}{KGN\ molar\ mass} = KGN\ load\ (mol)$$

$$\frac{KGN\ load\ (mol)}{Releasing\ volume\ (L)} = KGN\ concentration\ (M)$$

If KGN load is 5 µg and KGN molar mass is 317.3 g/mol,

$$KGN\ load\ (mol) = \frac{5 \times 10^{-6}\ g\ KGN}{317.3 \frac{g}{mol} KGN} = 1.5758 \times 10^{-8}\ mol\ KGN$$

$$KGN\ concentration\ (M) = \frac{1.5758 \times 10^{-8}\ mol\ KGN}{0.015\ L} = \mathbf{1.05053 \times 10^{-6}\ M\ KGN}$$

Consideration was then given to the KGN loading efficiency determined in preliminary study. Assuming a powder loading efficiency of 66%, the KGN load should increase from 5 µg KGN to 7.575 µg KGN per scaffold. This increase in loading compensates for the 33% loss of KGN that occurs in the fabrication process. The scaffolds are assumed to be 130 mg, calculated by multiplying the density of PLGA (1.3 g/cm^3) by the size of the scaffold (0.1 cm^3). Calculation for the updated ratio of KGN:PLGA in the powder mixture is shown below.

Since theoretical load is 5 µg KGN per 130 mg PLGA, but loading efficiency is 66%,

$$\frac{Theoretical\ load\ (ug)}{Loading\ efficiency} = Updated\ theoretical\ load\ (\mu g)$$

$$\frac{5\ ug\ KGN}{0.66} = 7.575\ \mu g\ KGN$$

Updated theoretical load is 7.575 µg KGN per 130 mg PLGA, find KGN:PLGA ratio:

$$\frac{7.575 \times 10^{-6} g\ KGN}{1.3 \times 10^{-3} g\ PLGA} = \mathbf{KGN{:}\ PLGA\ ratio\ of\ 1{:}17162}$$

3.2.2 Fabrication of PLGA-KGN Powder

PLGA with a PGA:PLA ratio of 50:50 and inherent viscosity of 1.03 dL/g was dissolved in DCM to create a 20% wt/vol solution. The dissolved PLGA was then combined with KGN at a KGN:PLGA ratio of 1:17162, as calculated in the previous section (KGN was first dissolved in 2 mL DMSO). The resulting PLGA-KGN mixture was stirred for 1 hr, then set in a fume hood overnight to evaporate most of the organic solvent. The next day, the mixture was heated at 75 ºC for 3-4 hours, then heated at 190 ºC for 30 min to remove any remaining DMSO. The resulting solid was then ground to a powder for use in bioprinting.

3.2.3 Bioprinting of PLGA-KGN Scaffolds

PLGA-KGN scaffolds were fabricated using the BioX bioprinter (CELLINK, Boston, MA). The scaffold's geometry (10 mm x 10 mm x 1 mm) was designed using SolidWorks 2019, and the inner pattern (rectilinear, 100% infill density, 0.33 mm layer height) was programmed using the BioX's integrated software. Primary PLGA-KGN powder was loaded into a metal cartridge and attached to a thermoplastic printhead. The print bed was lined with painter's tape to ensure adequate adhesion of the polymer. The loaded PLGA-KGN powder was melted at 150 ºC for 1 hr, then extruded at 400 kPa with an average speed of 2 mm/s using a 0.3 mm diameter nozzle. A preflow of 200 ms was also used during printing. Figure 3.1 shows the scaffold being printed.

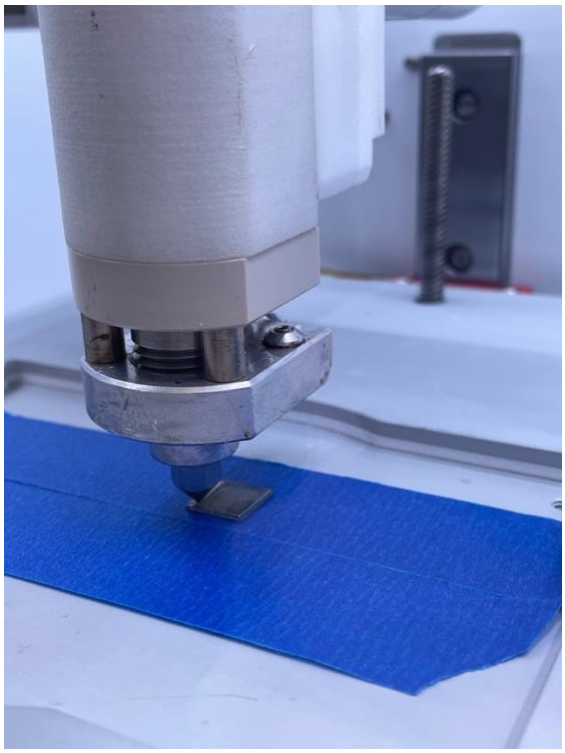

Figure 3.1 Bioprinting of PLGA-KGN scaffold

3.3 Determination of PLGA-KGN Scaffold Loading Efficiency

A PLGA-KGN scaffold was weighed and dissolved in 5 mL DMSO, and the released KGN concentration of the resulting solution was to be determined by high-pressure liquid chromatography (HPLC) using methyl hydroxide as the solvent. Unfortunately, the use of DMSO as a solvent for the PLGA-KGN scaffolds proved to be an impediment to HPLC readability, as it was not compatible with the HPLC column used. A solvent such as ethyl acetate should be used in the future, as it is more compatible with the column and could lead to more quantitative loading efficiency analysis.

3.4 Discussion

The PLGA-KGN scaffolds discussed in this chapter were produced using an updated fabrication protocol that included the addition of a DMSO evaporation step, as well as a modified KGN loading to reflect a therapeutic KGN dose. The loading efficiency of KGN into the scaffold was to be determined in order to understand the impact that the DMSO evaporation step has on these calculations. Though we were unable to obtain accurate results using our method of loading efficiency analysis, we strongly speculate that the addition of a DMSO evaporation step increased the scaffold's overall loading efficiency.

Previously, the bioprinting characteristics of preliminary PLGA-KGN powder were remarkably dissimilar from that of pure PLGA. It was concluded in the preliminary study that DMSO was present in the fabricated powder, indicating a need for a DMSO evaporation step. In printing the PLGA-KGN scaffolds discussed in this chapter, the bioprinting parameters and characteristics were identical to that of pure PLGA, suggesting that the majority (if not all) of DMSO had evaporated from the solid PLGA-KGN mixture prior to grinding to a powder. Overall, the addition of a DMSO evaporation step to the powder fabrication protocol allowed for a more predictable and controlled print and most likely improved loading efficiency calculations.

There were some limitations to the printing protocol that should be addressed in future study. Notably, though the PLGA-KGN material was much more predictable in its printing characteristics, there still remained some inconsistency between prints. For example, three PLGA-KGN scaffolds were printed using the same printing parameters, yielding printed masses of 95.4 mg, 94.4 mg, and 126.2 mg. Notably, none of the printed scaffolds yielded the theoretical scaffold mass of 130 mg. It is hypothesized that this inconsistency in scaffold mass highlights some error

in material extrusion and/or layer height, though this might largely be due to user error. A deeper understanding of bioprinting might help to resolve this issue in the future.

CHAPTER IV

DETERMINATION OF KGN RELEASE PROFILE

4.1 Overview

By design, KGN should demonstrate a biphasic release profile similar to other PLGA-encapsulated drugs. Initially, KGN located on the surface of the printed scaffold should readily diffuse into the surrounding solution. The second phase of KGN release should be dependent on bulk degradation of PLGA. As interior channels are created due to backbone cleavage of PLGA, KGN should diffuse from the interior of the scaffold into the surrounding solution.

A release experiment was conducted in order to establish the release characteristics of KGN from PLGA-KGN scaffolding. The findings of this study could demonstrate the potential of PLGA-KGN scaffolds as effective drug delivery vehicles. As discussed previously, modifications to PLA:PGA molar ratio, PLGA molecular weight, and other material characteristics of PLGA could influence the scaffold's degradation and subsequent KGN release, as could modifications to scaffold geometry and porosity. This affords the scaffold a tailored and customizable KGN release profile that is specific to patient needs.

4.2 Methods

Two PLGA-KGN scaffolds were printed and soaked in 15 mL sterile PBS at 37 ºC under gentle agitation. The supernatant was collected and replaced with fresh PBS every five days for 40 days. KGN concentration at the end of each time interval was determined by liquid chromatography-mass spectrometry (LC-MS). A preliminary PLGA-KGN scaffold was also soaked in 3 mL sterile PBS at 37º C under gentle agitation and was used in supernatant composition analysis.

4.3 Results and Discussion

The scaffolds gradually degraded over the 40-day period through a process of bulk erosion. By day 40, the scaffold was almost completely hydrolyzed. This degradation was visibly observed throughout the release study, as shown in Figure 4.1.

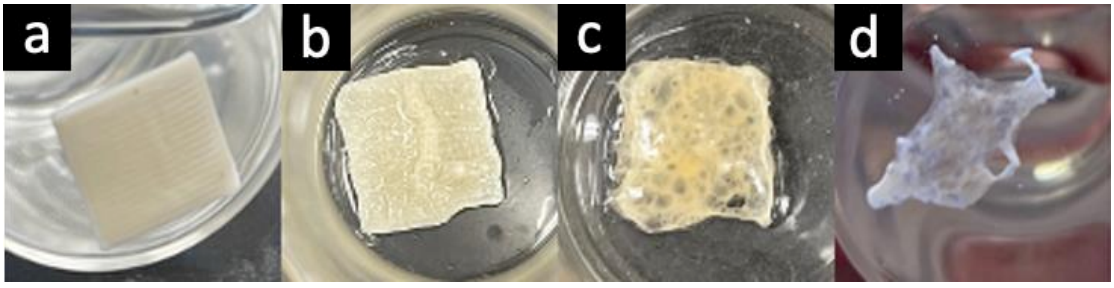

Figure 4.1 PLGA-KGN scaffolds at 5 days (a), 15 days (b), 25 days (c), and 35 days (d).

KGN concentration at each time interval was determined by LC-MS, and the resulting values were used to construct a release curve plotting cumulative KGN release as a function of time. At the time of writing, we had analyzed samples through day 25 and were in the process of analyzing samples from day 30 through day 40. The release profile of KGN from PLGA-KGN scaffolds is shown in Figure 4.2.

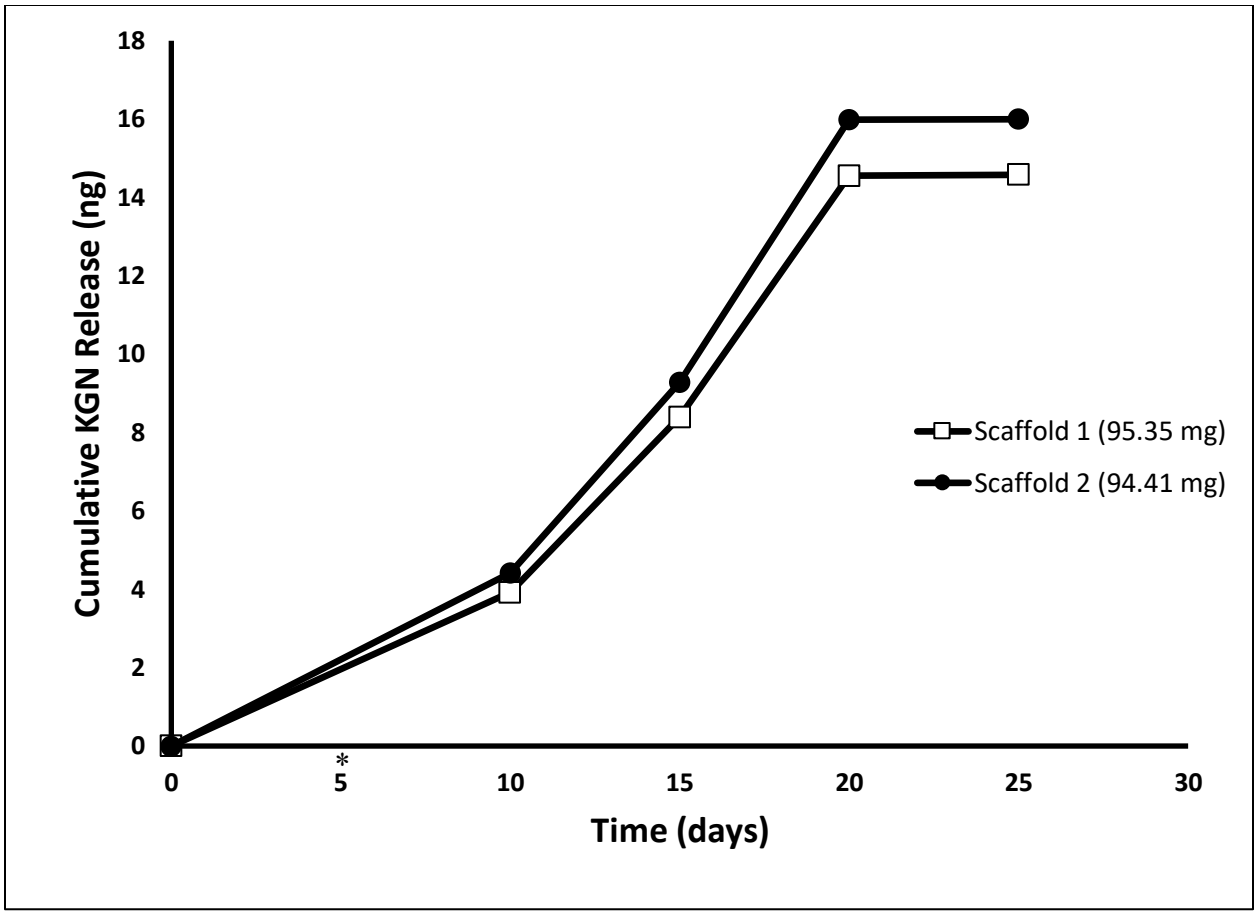

Figure 4.2 Release of KGN from PLGA-KGN scaffolds over 25 days.

**Note: Composition analysis was inconclusive for the 5-day time point. It is entirely possible that there was no release of KGN at this point, suggesting that KGN release is entirely dependent on PLGA hydrolysis.*

The results of this release experiment indicate that KGN undergoes a sustained release from PLGA-KGN scaffolds that occurs in tandem with PLGA hydrolysis, as evident in the biphasic release pattern indicated in Figure 4.2. A similar release pattern was observed in KGN release from the preliminary scaffold (data not shown). Notably, the cumulative mass of KGN released after 25 days is a much smaller value than expected. Assuming that 5 μg KGN was loaded for every 130 mg PLGA, the total percentage of loaded KGN released by Scaffold 1 (95.35 mg) and Scaffold 2 (94.41 mg) was 0.40% and 0.44%, respectively. This extremely low level of KGN

release indicates either a very poor loading efficiency or a degradation of KGN in solution over time. Since KGN loading was confirmed to be more than adequate in our preliminary study, we strongly speculate that KGN degraded in PBS over the course of the release experiment. To test this hypothesis, KGN degradation rate was studied in buffers of various pH levels. KGN was dissolved in buffers of 4.5, 7.3, and 10.3 pH, and KGN concentration was measured daily using HPLC. Findings indicate that a more acidic environment rapidly accelerates KGN degradation. A pH of 7.3, which is the pH of the sterile PBS that PLGA-KGN scaffolds were soaked in, facilitates KGN degradation in what appears to be a constant, linear progression. The results of this study are shown in Figure 4.3.

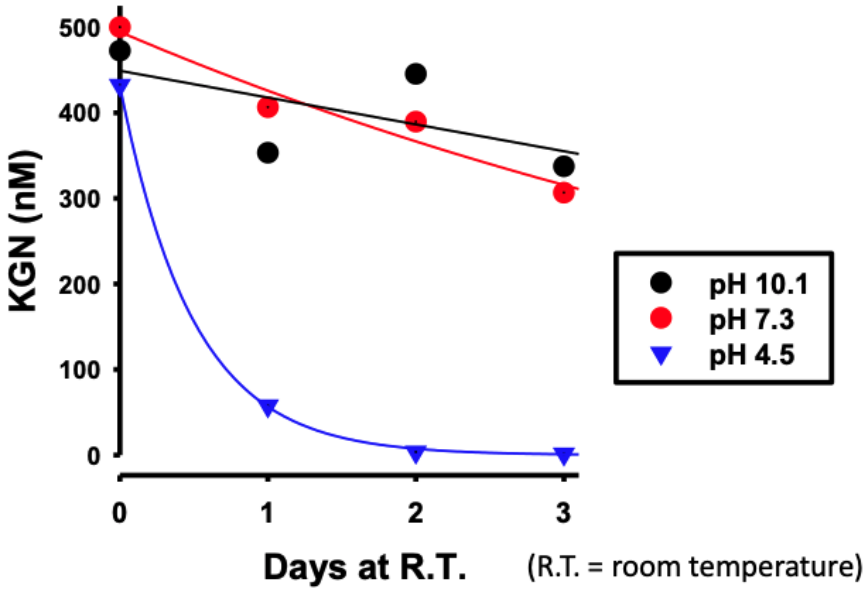

Figure 4.3 Degradation of KGN in buffers of various pH.

The proposed hydrolysis mechanism of KGN is shown in Figure 4.4. In aqueous solution, KGN degrades into 4-aminobiphenyl (4-ADP), phthalic anhydride, and phthalic acid.

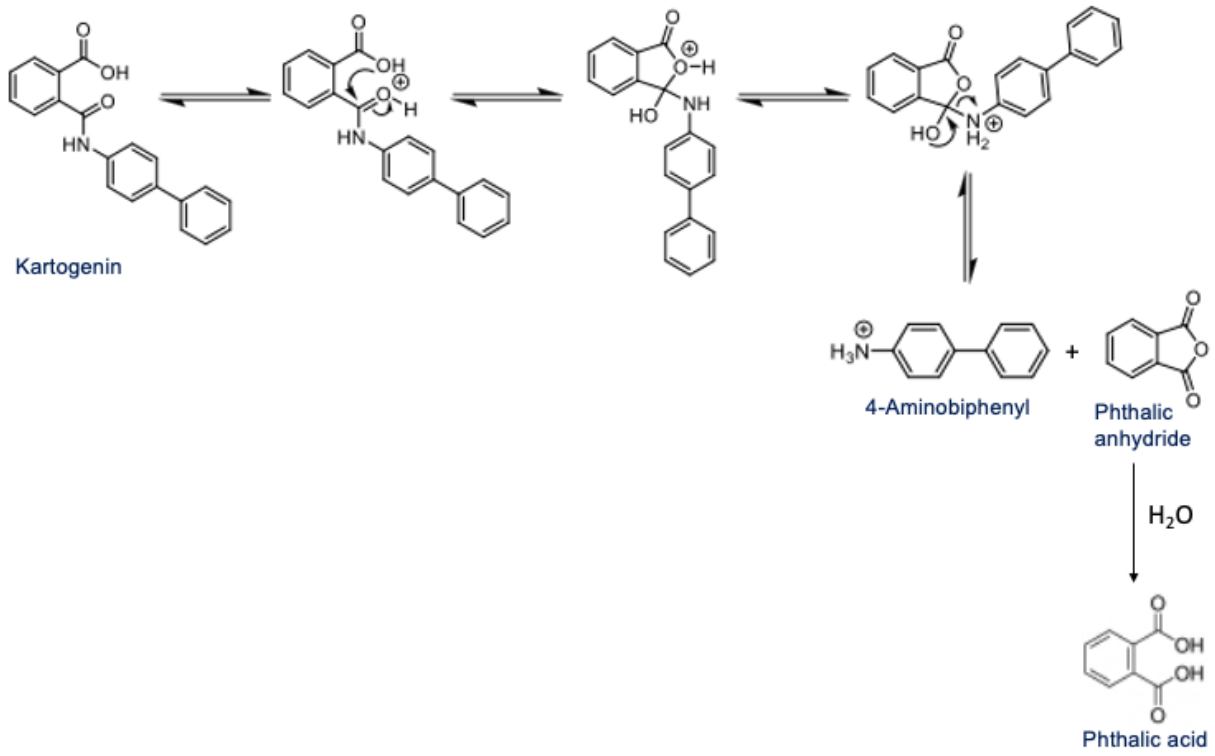

Figure 4.4 Proposed KGN degradation mechanism.

The day 10 supernatant of the soaked preliminary PLGA-KGN scaffold was evaluated by HPLC in order to determine its chemical composition. Rather than using primary scaffold samples, the preliminary scaffold was used due to its higher concentration of KGN loading, which allowed for more precise evaluation of its composition. HPLC-UV spectra for this sample at day 10 indicate the presence of KGN degradation products and the absence of KGN, shown in Figure 4.5a. The degradation products and KGN both feature the same biphenyl signature (shown in Figure 4.5b), which confirms that these are KGN products and not the result of contamination or other sources.

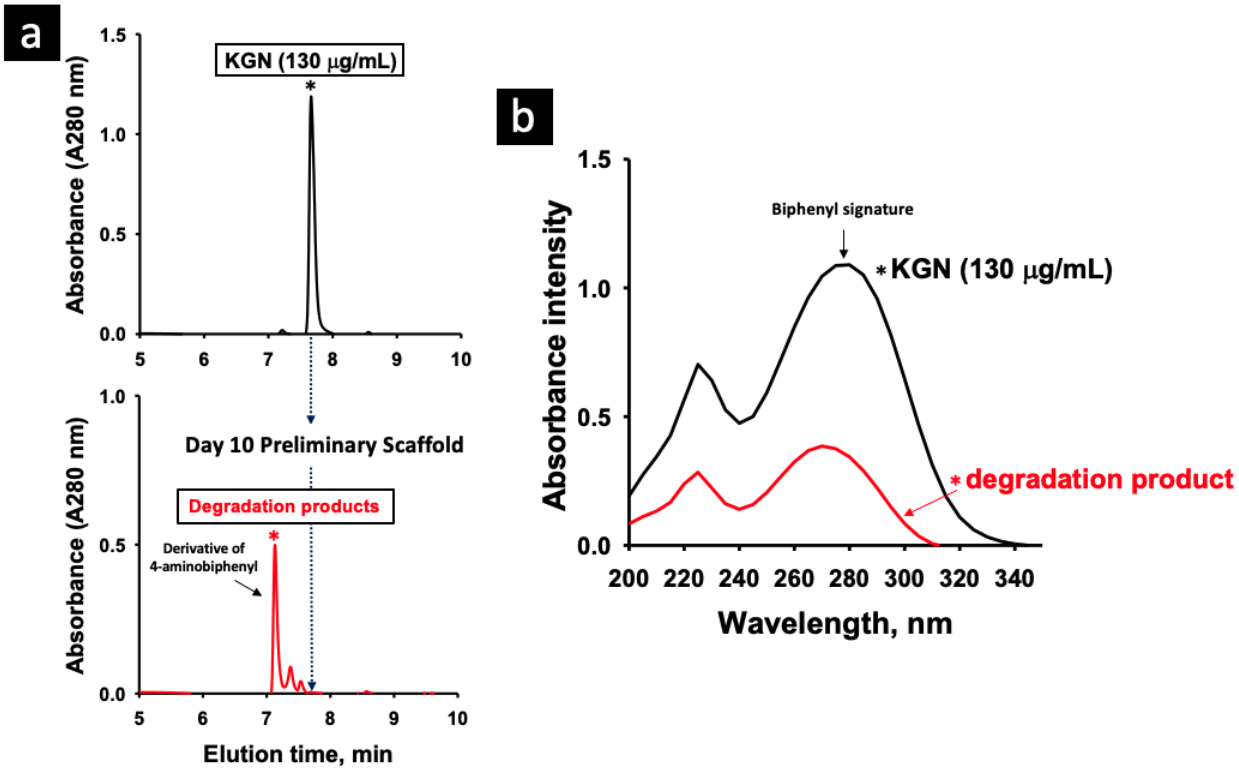

Figure 4.5 (a) Biphenyl signature of KGN and degradation products. (b) HPLC-UV chromatogram indicating presence of KGN degradation products at day 10.

The dominant peak in the HPLC-UV trace of the day 10 preliminary scaffold sample was determined to be 4'OH-4-ABP, an oxidation product of 4-ABP. Notably, studies have determined that the 4-ABP degradation product of KGN is the compound responsible for chondro-induction.[29] Therefore, the breakdown of KGN in solution by no means impacts the scaffold's chondro-inductive capacity. Although KGN degradation somewhat prevented us from quantifying KGN's exact release characteristics from PLGA-KGN scaffolds, we were still able to confirm a sustained release of KGN that is biphasic in nature and likely dependent on PLGA hydrolysis. This finding creates opportunities to modify the scaffold's chemical and physical design in order to fine-tune KGN release.

CHAPTER V

EFFECT OF KGN ON PLGA PRINT QUALITY

5.1 Overview

A PLGA-KGN scaffold used in this proposed application should have excellent mechanical properties, in order to withstand strong external loading conferred upon the knee joint. Therefore, it is important to determine the impact that the addition of KGN has on the mechanical properties of PLGA. KGN's mechanical influence was evaluated by performing mechanical tensile testing on printed tensile specimens. The impact of KGN on PLGA's elastic modulus, tensile strength, and toughness was then determined.

5.2 Bioprinting of Tensile Specimens

Tensile specimens were printed out of PLGA-KGN powder (as fabricated in Chapter III) and pure PLGA. The tensile specimens were designed in SolidWorks 2019, and the inner pattern (rectilinear, 100% infill, 0.33 mm layer height) was programmed using the BioX's integrated software. The print parameters of both samples are shown in Table 5.1. Figure 5.1 shows tensile specimens during and after bioprinting.

Table 5.1 Bioprinting Parameters of PLGA-KGN and PLGA Tensile Specimens

	PLGA-KGN	Control PLGA
Temperature	150 ℃	105 ℃
Pressure	400 kPa	192 kPa
Print Speed	9 mm/s	9 mm/s
Nozzle Size	0.4 mm	0.4 mm
Preflow	200 ms	200 ms

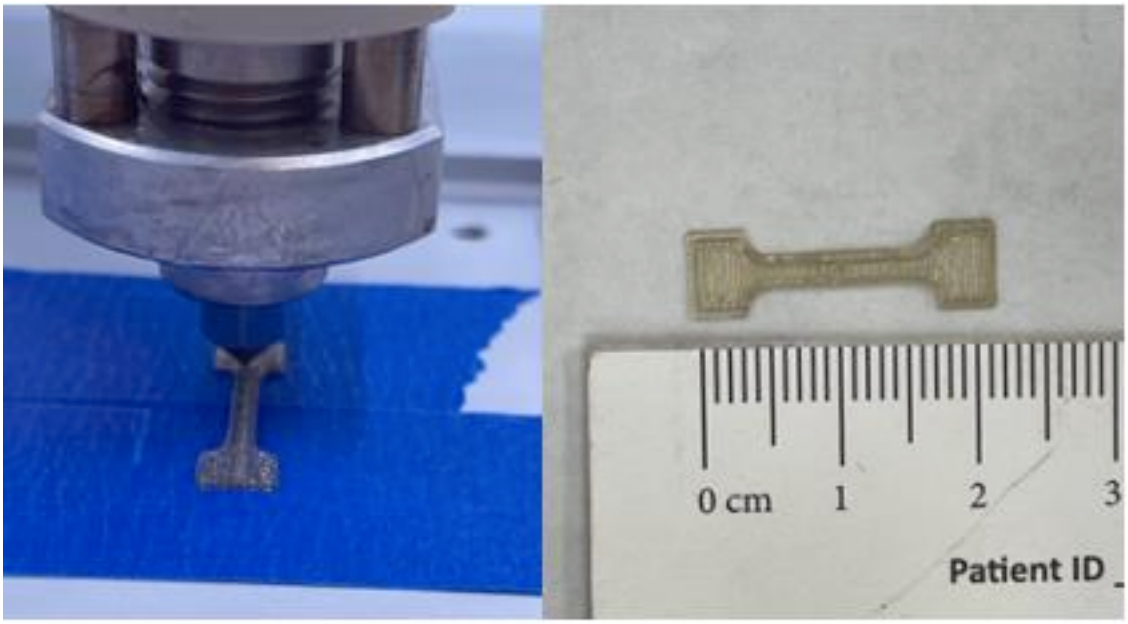

Figure 5.1 Bioprinting of tensile specimens.

5.3 Tensile Mechanical Testing Methods

Mechanical tensile testing was performed on the printed PLGA-KGN and PLGA tensile specimens (N=8 for PLGA-KGN, N=5 for control PLGA) using a Mach-1 stepper motor-driven micromechanical testing machine (Biomomentum, Quebec, Canada). All samples were stretched

at a displacement rate of 0.05 mm/s until specimen rupture (Fig. 5.2). Force vs. displacement data was recorded at a rate of 10 Hz. For each data point, tensile stress (Eq. 2) and strain (Eq. 3) were calculated based on the original dimensions of each specimen using the following equations.

$$\boldsymbol{\sigma} = \frac{F}{A} \tag{2}$$

Here, $\boldsymbol{\sigma}$ is tensile stress, F is applied tensile force to the specimen, and A is the cross-sectional area of the tensile specimen.

$$\boldsymbol{\varepsilon} = \frac{\Delta L}{L} \tag{3}$$

Here, $\boldsymbol{\varepsilon}$ is strain, ΔL is change in length, and L is undeformed length. In this case, ΔL corresponds directly to the obtained displacement values.

The elastic modulus was then determined by calculating the slope of the linear region of the stress-strain curve. Ultimate tensile strength was calculated by determining the maximum tensile stress value of the stress-strain curve. Toughness was also calculated by using trapezoidal approximation to determine the area beneath the stress-strain curve. Statistically significant differences in the calculated properties were determined by independent t-test (α=0.05).

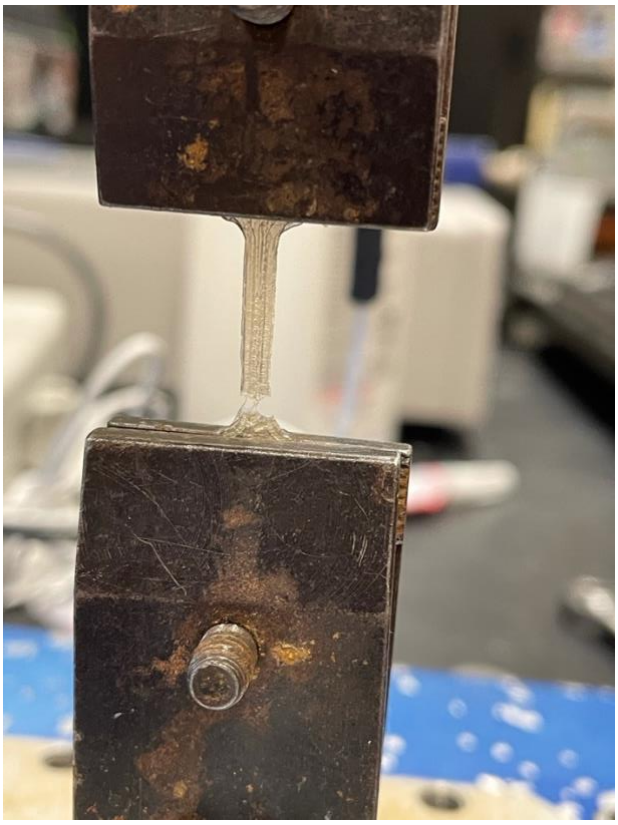

Figure 5.2 PLGA-KGN specimen rupture during tensile testing

5.4 Results and Discussion

In the printing of tensile specimens, there was an observable difference in bioprinting parameters between PLGA-KGN and pure PLGA. This is contrary to the previous finding that when properly fabricated, PLGA-KGN powder demonstrates identical print parameters to that of PLGA. There is reason to believe that the control PLGA powder was contaminated in some way, which resulted in its altered printing characteristics.

A stress-strain curve was constructed using the results of tensile testing, shown in Figure 5.3.

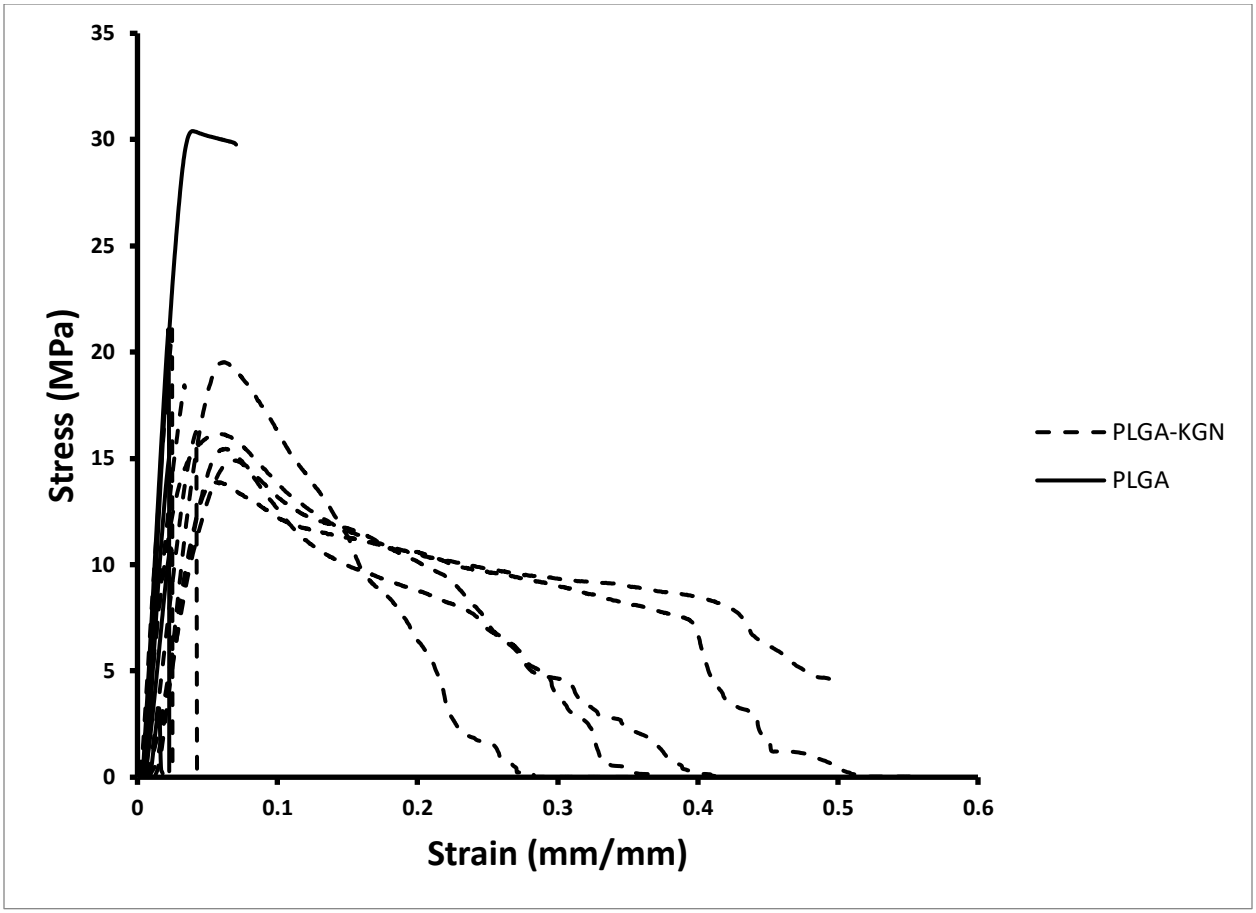

Figure 5.3 Tensile stress vs strain of printed PLGA-KGN and PLGA specimens.

Elastic modulus calculations were determined by calculating the slope of each sample's linear region. No significant difference in elastic modulus ($p>0.05$) was observed between PLGA-KGN and control PLGA. Ultimate tensile strength was determined by calculating the maximum tensile stress tolerated by each sample. No significant difference in tensile strength ($p>0.05$) was observed between PLGA-KGN and control PLGA. Material toughness was determined by trapezoidal approximation of the area beneath each sample's stress-strain curve. There was an observed difference in average toughness between PLGA-KGN and control PLGA, with PLGA-KGN exhibiting a significantly higher average toughness ($p<0.05$). Figures 5.4, 5.5, and 5.6

respectively show elastic modulus, tensile strength, and toughness of the two materials obtained by tensile testing.

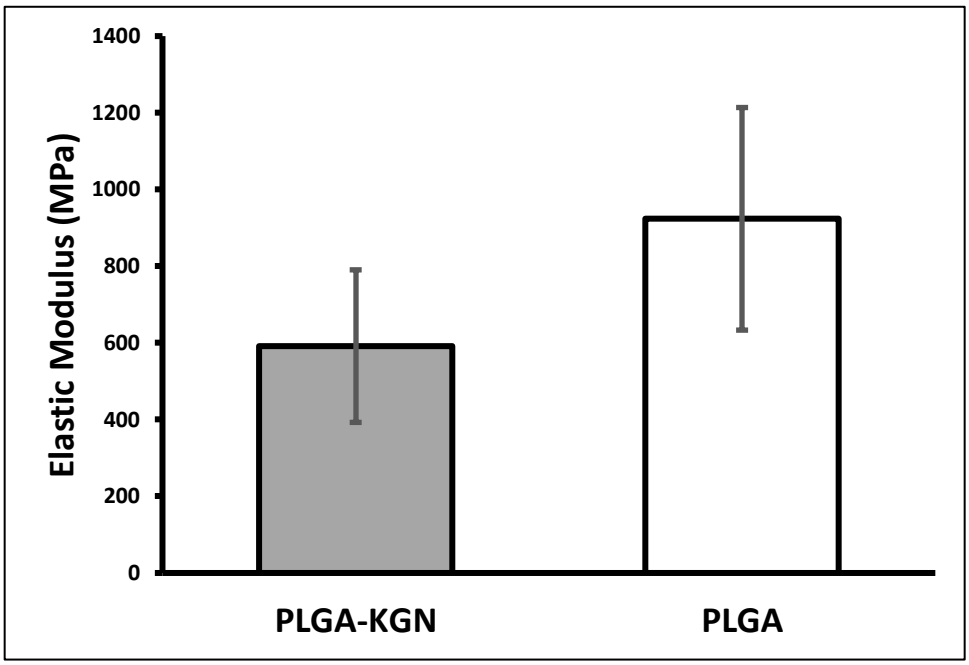

Figure 5.4 Average elastic modulus (mean +/- stdev) of printed PLGA-KGN and PLGA specimens (p-value = 0.063).

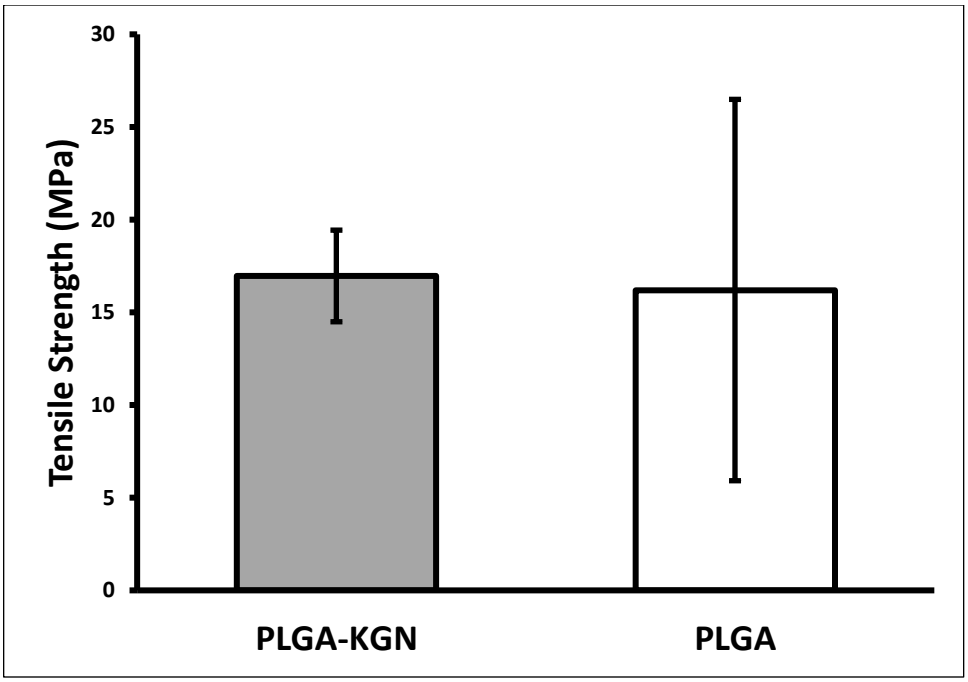

Figure 5.5 Average tensile strength (mean +/- stdev) of printed PLGA-KGN and PLGA specimens (p-value = 0.88).

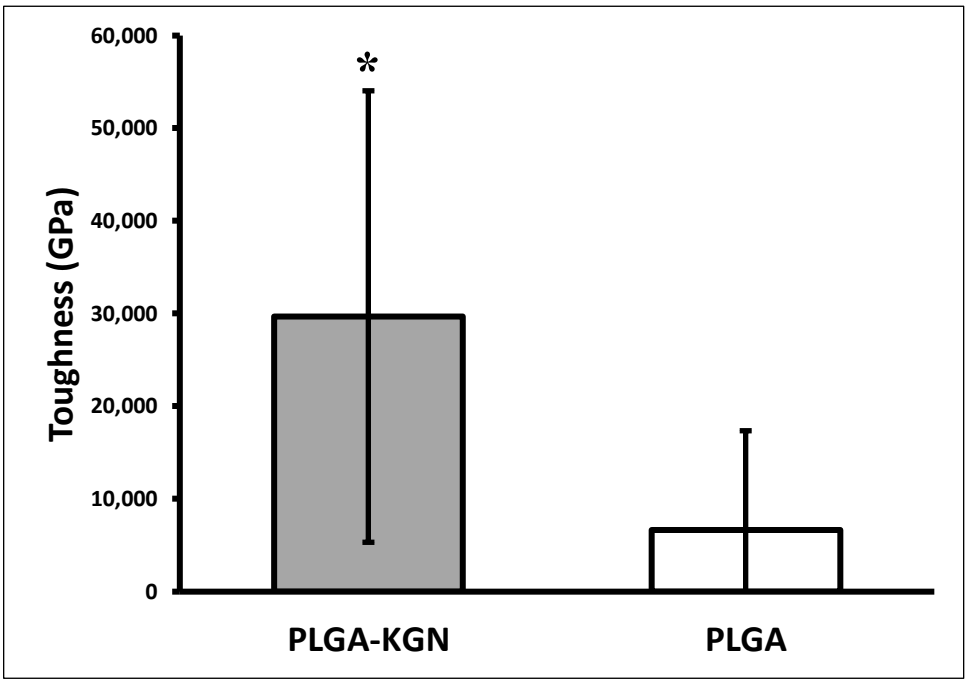

Figure 5.6 Average toughness (mean +/- stdev) of printed PLGA-KGN and PLGA specimens (*p-value <0.05).

The results of the mechanical testing study indicate that the addition of KGN does not negatively impact the mechanical properties of PLGA. KGN was observed to have no impact on PLGA's elastic modulus or tensile strength, but PLGA-KGN did exhibit an increased toughness when compared to control PLGA. This indicates that PLGA-KGN can absorb more strain energy prior to rupture than PLGA.

CHAPTER VI

CONCLUSIONS

6.1 Summary

The results of this study lead to several promising conclusions. Our preliminary analysis of KGN loading efficiency confirms KGN's ability to be loaded into a PLGA-KGN scaffold and its ability to withstand the high temperatures and pressures associated with the bioprinting process. The PLGA-KGN powder fabrication and bioprinting process was further validated by printing PLGA-KGN scaffolds with a therapeutic KGN loading dose. These scaffolds were soaked in sterile PBS over 40 days in order to determine KGN release profile. The findings of this study confirm a sustained release of KGN from PLGA-KGN scaffolds occurring in tandem with PLGA hydrolysis. Further work will aim to better quantify KGN release now that there is a greater understanding of how KGN degrades in solution. Results of mechanical testing indicate that the inclusion of KGN is not detrimental to PLGA's mechanical properties. In fact, the increased fracture toughness of functionalized PLGA further increases the scaffold's ability to withstand joint loading. Overall, these findings suggest that this method of scaffold fabrication and functionalization is a very viable option for delivering KGN to defect sites immediately after microfracture. This augmentation to microfracture has the potential to overcome the limitations of the procedure and promote the regeneration of healthy, functional cartilage in patients with osteoarthritis.

6.2 Future Work

Further work on this project will aim to confirm the chondrogenic activity of released kartogenin in vitro using primary marrow-derived mesenchymal stem cells. These cells have been acquired and are currently undergoing expansion. Chondrogenic influence of the proposed augmentation will also be evaluated in vivo using a rat knee model of knee microfracture.

REFERENCES

1. Mandelbaum, B. R. *et al.* Articular cartilage lesions of the knee. *Am. J. Sports Med.* (1998). doi:10.1177/03635465980260062201

2. OUTERBRIDGE, R. E. The etiology of chondromalacia patellae. *J. Bone Joint Surg. Br.* **43-B**, 752–757 (1961).

3. Browne, J. E. & Branch, T. P. Surgical alternatives for treatment of articular cartilage lesions. *The Journal of the American Academy of Orthopaedic Surgeons* **8**, 180–189 (2000).

4. Widuchowski, W., Widuchowski, J. & Trzaska, T. Articular cartilage defects: Study of 25,124 knee arthroscopies. *Knee* **14**, 177–182 (2007).

5. Heir, S. *et al.* Focal cartilage defects in the knee impair quality of life as much as severe osteoarthritis: A comparison of knee injury and osteoarthritis outcome score in 4 patient categories scheduled for knee surgery. *Am. J. Sports Med.* **38**, 231–237 (2010).

6. Gowd, A. K. *et al.* Management of Chondral Lesions of the Knee: Analysis of Trends and Short-Term Complications Using the National Surgical Quality Improvement Program Database. *Arthrosc. - J. Arthrosc. Relat. Surg.* **35**, 138–146 (2019).

7. Litwic, A., Edwards, M. H., Dennison, E. M. & Cooper, C. Epidemiology and burden of osteoarthritis. *Br. Med. Bull.* **105**, 185–199 (2013).

8. Johnson, K. *et al.* A stem cell-based approach to cartilage repair. *Science (80-.).* (2012). doi:10.1126/science.1215157

9. Madry, H. *et al.* Early osteoarthritis of the knee. *Knee Surgery, Sports Traumatology, Arthroscopy* **24**, 1753–1762 (2016).

10. Ding, C. *et al.* Natural history of knee cartilage defects and factors affecting change. *Arch. Intern. Med.* **166**, 651–658 (2006).

11. Ding, C., Cicuttini, F., Scott, F., Boon, C. & Jones, G. Association of prevalent and incident knee cartilage defects with loss of tibial and patellar cartilage: A longitudinal study. *Arthritis Rheum.* **52**, 3918–3927 (2005).

12. Steadman, J. R., Rodkey, W. G. & Briggs, K. K. Microfracture: Its history and experience of the developing surgeon. *Cartilage* **1**, 78–86 (2010 13. Mithoefer, K., Mcadams, T., Williams, R. J., Kreuz, P. C. & Mandelbaum, B. R. Clinical efficacy of the microfracture technique for articular cartilage repair in the knee: An evidence-based systematic analysis. *American Journal of Sports Medicine* (2009). doi:10.1177/0363546508328414

13. Mithoefer, K., Mcadams, T., Williams, R. J., Kreuz, P. C. & Mandelbaum, B. R. Clinical efficacy of the microfracture technique for articular cartilage repair in the knee: An evidence-based systematic analysis. *American Journal of Sports Medicine* (2009). doi:10.1177/0363546508328414

14. Orth, P., Gao, L. & Madry, H. Microfracture for cartilage repair in the knee: a systematic review of the contemporary literature. *Knee Surgery, Sports Traumatology, Arthroscopy* (2020). doi:10.1007/s00167-019-05359-9

15. Frisbie, D. D. *et al.* Early events in cartilage repair after subchondral bone microfracture. *Clin. Orthop. Relat. Res.* **407**, 215–227 (2003).

16. Peterson, L., Brittberg, M., Kiviranta, I., Åkerlund, E. L. & Lindahl, A. Autologous chondrocyte transplantation: Biomechanics and long-term durability. *Am. J. Sports Med.* **30**, 2–12 (2002).

17. Kaul, G., Cucchiarini, M., Remberger, K., Kohn, D. & Madry, H. Failed cartilage repair for early osteoarthritis defects: A biochemical, histological and immunohistochemical analysis of the repair tissue after treatment with marrow-stimulation techniques. *Knee Surgery, Sport. Traumatol. Arthrosc.* **20**, 2315–2324 (2012).

18. Krych, A. J., Saris, D. B. F., Stuart, M. J. & Hacken, B. Cartilage Injury in the Knee: Assessment and Treatment Options. *J. Am. Acad. Orthop. Surg.* **28**, 914–922 (2020).

19. Douleh, D. & Frank, R. M. Marrow Stimulation: Microfracture, Drilling, and Abrasion. *Oper. Tech. Sports Med.* **26**, 170–174 (2018).

20. Goyal, D., Keyhani, S., Lee, E. H. & Hui, J. H. P. Evidence-based status of microfracture technique: A systematic review of Level I and II studies. *Arthroscopy - Journal of Arthroscopic and Related Surgery* **29**, 1579–1588 (2013).

21. Connelly, J. T., García, A. J. & Levenston, M. E. Interactions between integrin ligand density and cytoskeletal integrity regulate BMSC chondrogenesis. *J. Cell. Physiol.* **217**, 145–154 (2008).

22. Stevens, M. M. Biomaterials for bone tissue engineering. *Materials Today* **11**, 18–

25 (2008).

23. Gentile, P., Chiono, V., Carmagnola, I. & Hatton, P. V. An overview of poly(lactic-co-glycolic) Acid (PLGA)-based biomaterials for bone tissue engineering. *International Journal of Molecular Sciences* **15**, 3640–3659 (2014).

24. Lee, P. W. & Pokorski, J. K. Poly(lactic-co-glycolic acid) devices: Production and applications for sustained protein delivery. *Wiley Interdisciplinary Reviews: Nanomedicine and Nanobiotechnology* (2018). doi:10.1002/wnan.1516

25. He, Y. & Lu, F. Development of Synthetic and Natural Materials for Tissue Engineering Applications Using Adipose Stem Cells. *Stem Cells International* (2016). doi:10.1155/2016/5786257

26. Makadia, H. K. & Siegel, S. J. Poly Lactic-co-Glycolic Acid (PLGA) as biodegradable controlled drug delivery carrier. *Polymers (Basel)*. **3**, 1377–1397 (2011).

27. Guo, T. *et al.* 3D printed biofunctionalized scaffolds for microfracture repair of cartilage defects. *Biomaterials* (2018). doi:10.1016/j.biomaterials.2018.09.022

28. Xu, X. *et al.* Full-thickness cartilage defects are repaired via a microfracture technique and intraarticular injection of the small-molecule compound kartogenin. *Arthritis Res. Ther.* (2015). doi:10.1186/s13075-015-0537-1

29. Zhang, S. *et al.* Kartogenin hydrolysis product 4-aminobiphenyl distributes to cartilage and mediates cartilage regeneration. *Theranostics* **9**, 7108–7121 (2019).